Measuring the number and spacing of molecular motors propelling a gliding microtubule

Todd L. Fallesen, Jed C. Macosko, and G. Holzwarth

Phys. Rev. E **83**, 011918 — Published 28 January 2011

DOI: 10.1103/PhysRevE.83.011918

Measuring the number and spacing of molecular motors propelling a gliding microtubule

*Todd L. Fallesen, Jed C. Macosko, and G. Holzwarth**

Department of Physics, Wake Forest University, Winston-Salem, NC 27109

* Correspondence: gholz@wfu.edu

G. Holzwarth, Department of Physics, Wake Forest University, PO Box 7507

Winston-Salem, NC 27109

ABSTRACT:

The molecular motor gliding assay, in which a microtubule or other filament moves across a surface coated with motors, has provided much insight into how molecular motors work. The kinesin-microtubule system is also a strong candidate for the job of nanoparticle transporter in nanotechnology devices. In most cases, several motors transport each filament. Each motor serves both to bind the microtubule to a stationary surface and to propel the microtubule along the surface. By applying a uniform transverse force of 4-19 pN to a superparamagnetic bead attached to the trailing end of the microtubule, we have measured the distance *d* between binding points (motors). The average value of *d* was determined as a function of motor surface density σ. The measurements agree well with the scaling model of Duke, Holy, and Liebler, which predicts that $\langle d \rangle \sim \sigma^{-2/5}$ if $0.05 \le \sigma \le 20\ \mu\text{m}^{-2}$ [Physical Review Letters 74, 330-333(1995)]. The distribution of *d* fits an extension of the model. The radius of curvature of a microtubule bent at a binding point by the force of the magnetic bead was ≈1 μm, 5000-fold smaller than the radius of curvature of microtubules subjected only to thermal forces. This is evidence that at these points of high bending stress, generated by the force on the magnetic bead, the microtubule is in the more flexible state of a two-state model of microtubule bending proposed by Heussinger, Schüller and Frey [Phys. Rev. E 81, 021904(2010)].

PACS numbers: 87.16.Nn, 87.80.Nj

I. INTRODUCTION

Gliding assays of motor proteins such as kinesin have provided much insight into how molecular motors work[1, 2]. There is also increasing interest in using gliding microtubules as molecular shuttles[3-6]. Two key parameters for both these areas are the number of motors n pulling the microtubule, and the distance d between the motors. For a microtubule of length L, $n \approx L/d$. The parameter d is expected to affect cooperation between motors.

The experimental determination of d or n in gliding assays, in bead assays, and *in vivo* remains problematic. In gliding assays, the presence of only one motor can be established if the microtubule is observed to swivel about a single binding point[7]. However, if the microtubule does not swivel, the number of active motors is not readily apparent. Microtubule velocity can serve as an approximate metric for n provided there is significant load per motor [8].

In bead assays, beads with 1, 2, or 3 functional motors can be prepared by changing the concentration of the kinesin solution in which the beads are incubated[9]. The functional number on a particular bead has been inferred from the stall force of the bead in an optical trap [10]. An alternative approach is to use dynamic light scattering to estimate the average number of motors bound to each bead, and then to determine the fraction of this average which, from geometric considerations, could bind to a nearby microtubule [11]. The number

of motors pulling a cargo *in vivo* has been estimated from both stall force [12-14] and cargo velocity [15-18].

In this paper, we directly determine the separation distance *d* between motors bound to a gliding microtubule. Since the length *L* of a microtubule is easily measured, *d* provides another route to *n.* It is easy to control the *relative* number of kinesin motors in a flow chamber. If *N* molecules are injected and all the injected motors bind to the surface of the chamber, the nominal surface density of motors is given by $\sigma_{nom} = N/A$, where *A* is the surface area. Alternatively, the surface density can be measured by reflectometric interference spectroscopy[19]. However, of the total number of motors bound to the surface, only a fraction, roughly 10%, are functional[20]. The surface density σ of these functional motors can be estimated from the landing rate of microtubules on a kinesin-coated surface[21, 22]. However, the scaling relation between σ and *n* remains untested and is not expected to be simply $n \sim \sigma$, although this is sometimes assumed.

As a microtubule glides over a kinesin-coated surface, the number of motors decreases by one whenever a bound motor reaches the trailing end of the microtubule. Meanwhile, motors add at the leading end of the microtubule. How often will that occur? In a theoretical paper, Duke, Holy and Liebler (DHL) suggest that "As the microtubule moves ahead, its leading end fluctuates laterally, so that when it has advanced a distance *l* from the position of the most recently bound motor, it will have explored an area *A(l)* of the surface." [23] Assuming a diffusion-limited interaction between the microtubule and the kinesin molecules

available within area A, they suggest that the dependence of A on l breaks into three scaling regimes:

Regime i arises with high kinesin surface density. The microtubule will encounter another kinesin quickly, so the tip length l is short. Like a short cantilever, the tip does not bend significantly. However, the heads of each kinesin motor are connected to the glass surface through an 80 nm coiled-coil, which gives the heads some lateral freedom of motion. so only motors located within a distance $w/2$ from the center of the path of the advancing microtubule can attach to it. Thus $A \sim wl$. Based on the length of the kinesin stalk, DHL suggest that $w \approx 20$ nm.

Regime ii is defined by values of l for which the microtubule tip is long enough to bend significantly. Assuming the tip bends like a cantilever, $A \sim l^2\theta$, where θ is the angle through which it bends due to thermal agitation. Since $\theta \sim (l/p)^{1/2}$, where p is the persistence length of the microtubule, one obtains $A \sim l^{5/2}p^{-1/2}$.

Regime iii occurs when l is so long that the motion of the tip is limited by viscous damping of its bending motion. In regime iii, $A \sim (\gamma/v)^{1/2}$, where γ is the friction factor for rotational motion of the microtubule and v is the velocity of the microtubule.

The mean distance $\langle d \rangle$ between bound motors, which we measure in this paper, is specified in the DHL model by the condition,

$$\sigma A(l = \langle d \rangle) = 1 \qquad (1)$$

The scaling behavior of $\langle d \rangle$ with σ then becomes[23]:

$$\langle d \rangle \sim \sigma^{-1} w^{-1}, \qquad \sigma >> \sigma^{*} \ , \qquad \text{Regime i} \qquad (2a)$$

$$\langle d \rangle \sim \sigma^{-2/5} p^{1/5} \qquad \sigma^{*} >> \sigma >> \sigma^{**}, \ \text{Regime ii} \qquad (2b)$$

$$\langle d \rangle \sim \sigma^{-1} \left(\gamma / \nu \right)^{-1/2} \qquad \sigma^{**} >> \sigma, \qquad \text{Regime iii} \qquad (2c)$$

Note that $\langle d \rangle$ scales differently with σ in regimes i and ii.

A diagram showing how the searched area *A* increases with *l* is shown in Fig. 1. Within this diagram, it is useful to consider the fate of a tip as it extends with a velocity *v* from its nearest binding point. First it must pass through regime i. If σ is large, there is a high probability that the tip finds a motor in regime i. The value of $\langle d \rangle$ is then small. Once it finds a motor, *l* resets to 0. However, if σ is small, the tip is likely to pass through regime i without finding a motor. Upon reaching regime ii, the probability of finding a motor increases since

dA/dl increases. If the tip finds a motor in regime ii, $\langle d \rangle$ is larger than it would

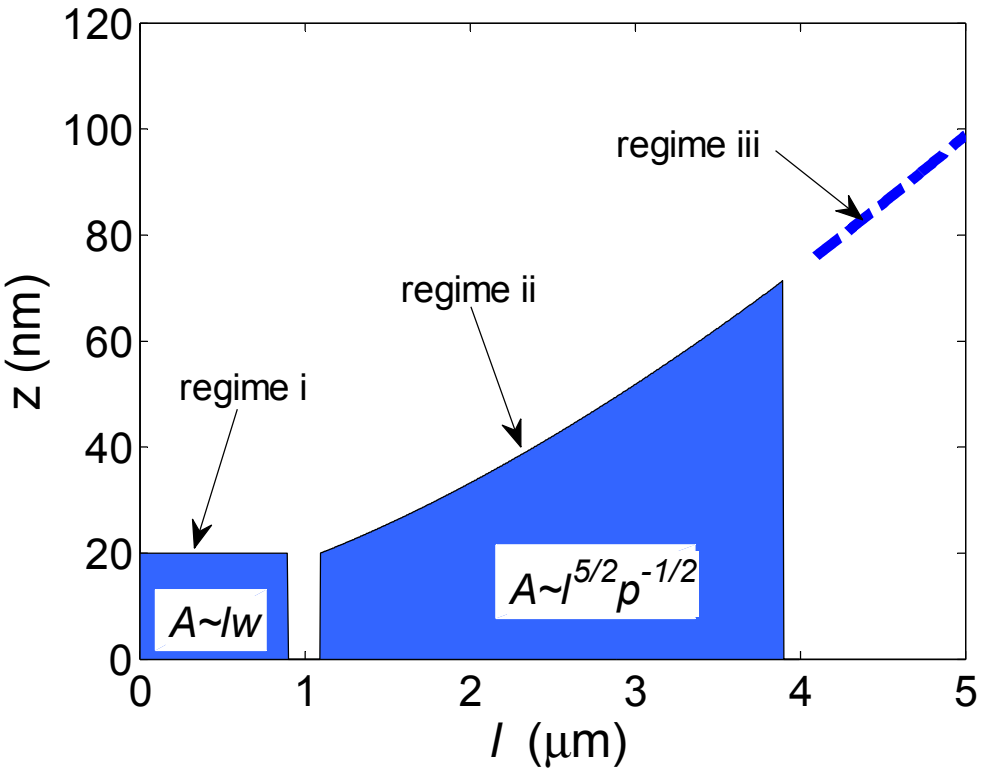

FIG. 1. The three regimes of the DHL model. Although we have set the boundaries between the regimes at 1μm and 4μm, these actually depend upon σ.

be for a motor found in regime i. Finally, if the tip reaches regime iii, even larger values of $\langle d \rangle$ will occur.

The two values of σ which define the boundaries between the 3 regimes, designated σ^* and σ^{**} in Eq. (2), are estimated by DHL to be given by $\sigma^* \approx 20 \mu m^{-2}$ and $\sigma^{**} \approx 0.05 \mu m^{-2}$. The scaling behavior of <*d*> with σ is untested.

To test the scaling behavior of the model, we have measured $\langle d \rangle$ over a 5-fold range in σ. Gliding assays were carried out in the presence of a magnetic field which applied 4-19 pN force to a superparamagnetic bead attached to the (+) end of the microtubule[24]. If the direction of this force was 90° to the long axis of the microtubule, the microtubule experienced a bending moment of order 20 pN·μm. This exceeded the torques of random thermal motions by a factor of approximately 1000. The microtubule was observed to bend sharply around an apparent binding point fixed on the surface. If the transverse magnetic force remained on, the microtubule detached abruptly from the first binding point after 1-2s, revealing the next binding point as a new sharp bend at a different location on the surface. This process continued as the microtubule became detached from its initially invisible binding points one after another. We take the distance between these binding points as *d,* the distance between motors bound to the microtubule. A recent study of the microtubule bending under perpendicular electric forces has measured *d* from deflections of the front end, rather than the trailing end, of the microtubule[25].

In addition to testing the scaling behavior of $\langle d \rangle$ predicted by the DHL theory, our experiments lend support to the largely untested molecular model of microtubule bending developed by Heussinger and coworkers [26, 27].

II. EXPERIMENTAL METHODS

Full-length *D. melanogaster* kinesin-1 was prepared from plasmid pPK113 as described by Coy [28]. The concentration of the purified protein was 94μg/mL, based on A_{280} and ε_{280} = 42915 $M^{-1}cm^{-1}$. SDS-page analysis showed a single band at 115±5kDa, the expected value. The kinesin was flash frozen in liquid nitrogen and stored at -80C.

Fluorescently labeled microtubules with short biotin labeled tails at their (+) ends were prepared in two stages as previously described[8, 29]. In the first step, 14% rhodamine labeled bovine tubulin was copolymerized with 86% unlabeled bovine tubulin (Cytoskeleton, Denver CO) for 45 minutes at 37C, giving long, fluorescent microtubules. In the second step, biotin labeled bovine tubulin (Cytoskeleton) was added and the sample was incubated for an additional 15 minutes at 37C. This step added short, biotin-labeled tails to the (+) ends of the pre-existing microtubules. Conveniently, the biotin-labeled tails were weakly fluorescent but still detectable compared to the more intensely fluorescent main portion of each microtubule.

Upside down gliding assays were performed in rectangular glass capillaries, 0.5mm x 0.05mm x 25mm (Vitrocom, Mountain Lakes, NJ). A solution consisting of 0.5mg/ml casein (Fisher, Atlanta, GA) in BRB80 (80mM PIPES buffer, 1mM EGTA, 1mM $MgCl_2$, pH 6.9) (Sigma-Aldrich, St. Louis, M0) was flowed into the capillary to coat its inner surfaces. After 5 minutes, a solution of BRB80 supplemented with 1mM Mg-ATP and 1.5-8.4μg/ml kinesin

was injected into the capillary. The full-length kinesin molecules became bound to the casein-coated surfaces, presumably by their tails[30]. Following this, a solution containing BRB80, 1mM Mg-ATP, 30μM taxol, 5mM $MgCl_2$, 40mM D-glucose, 0.02mg/ml catalase, 0.04mg/ml glucose oxidase, 60mM beta-mercaptoethanol, 0.002% tubulin (as microtubules) and 0.0375% streptavidin-coated, 2.8μm diameter polystyrene superparamagnetic beads (M270, Invitrogen, Carlsbad, California) was flowed into the capillary. Some of the streptavidin-labeled beads became attached to the biotin-labeled tails of the microtubules. In most cases only a single bead attached itself. The open ends of the capillary tube were then sealed with biologically inert grease (Mobil FM102, Exxon-Mobil, Houston, TX) and the capillary was placed into the gap of an electomagnet which fitted into our microscope.

The microscope used was a Nikon Eclipse 6000FN microscope equipped with a 60X water immersion objective, a rhodamine fluorescence cube, and a CCD camera (Hamamatsu ORCA 4742-95-12ER, Hamamatsu, Japan). The electromagnet, which replaced the standard microscope stage, could apply a 4-19pN force to the beads. The pole pieces of the electromagnet were shaped to provide a uniform magnetic force on the beads over a 6mm length of the capillary tube [24].

The nominal surface density of the motors, σ_{nom}, was calculated by assuming that every motor injected into the capillary became adsorbed to the casein-coated inside surface of the capillary. For a capillary of width W, and height H, $\sigma_{nom} = \frac{WH[K]N_A}{2(W+H)M}$, where [K] is the concentration in g/L of injected kinesin, M is the molecular weight of the kinesin heavy chain dimer, 230,000 Da, and N_A is Avogadro's number.

III. RESULTS

A. Detachment of microtubule from anchor points.

When the magnet current was turned on, the bead felt a force $\mathbf{F} = \nabla(\mathbf{m} \cdot \mathbf{B})$, where **m** is the magnetic moment of the bead and **B** is the magnetic field. Our experiments were done with a superparamagnetic bead in a field exceeding 0.1T. Under these conditions *m* saturates so $\mathbf{F} = m\nabla\mathbf{B}$ [24]. Our magnet had a wedge-shaped gap. Although **B** pointed from one pole to the other, $\nabla\mathbf{B}$ and $\mathbf{F}$ pointed from the wide end of the gap to the narrow end. The gap was shaped so that *F* was constant, greatly simplifying the interpretation of the experiments. The long axis of the capillary was aligned parallel to the direction of **F**.

Microtubules were observed to glide in all directions. If a microtubule was gliding perpendicular to $\mathbf{F}$, we frequently observed that the microtubule bent sharply around a point fixed on the coverslip surface, but continued to move around the fixed point like a rope going over a pulley attached to a wall. We call this fixed point an "anchor point" (see Figs 2, 3 and two supplemental movies available on EPAPS [31]). As the microtubule continued to glide around the anchor point, it abruptly detached from the anchor point after ≈1s, provided the transverse force on the bead was greater than 4pN. After detachment, the bead moved rapidly in an arc around the next anchor point, pulling the newly released section of the microtubule behind it (Figs 2 and 3). The magnetic force detached the microtubule from its anchor points

one-after-another until the microtubule swiveled about the anchor point. This signaled that the microtubule was attached by only one motor[7]. The detachment process can be is best observed in the supplemental movies[31]. The leading tip of the microtubule maintained an average velocity of 660nm/s throughout the experiment, although the velocity decreased briefly immediately after detachments.

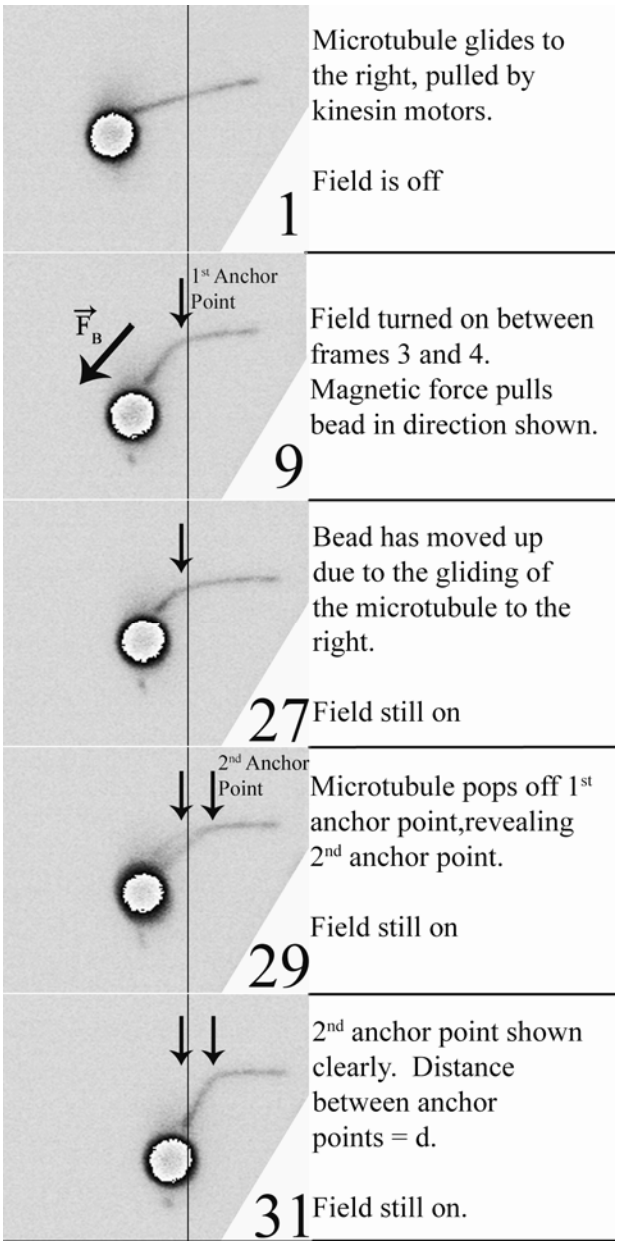

FIG 2. Image sequence during a gliding assay showing two anchor points and one detachment event. The microtubule was gliding to the right throughout the sequence. The magnetic field was off in frame 1-3. After frame 3, a 1.4A current was applied to the magnet.

The resultant magnetic field applied a 4 pN force to the magnetic bead[24]. The direction of the force on the magnetic bead is shown in frame 9. The first anchor point is visible in frame 9 and is marked with an arrow. Between frames 9 and 27, attached kinesin motors continue to pull the microtubule to the right. This pulls the attached bead upward toward the 1st binding point. During frame 29 the microtubule detaches from the 1st anchor point and begins to show the location of the 2nd second anchor point. The two arrows in frame 29 mark the locations of the 1st and 2nd anchor points. The distance between the anchor points is *d*. The bead diameter, 2.8μm, serves as an internal length scale in all frames. The images in this figure are part of Popoff_movie_1.avi which can be seen on EPAPS[31].

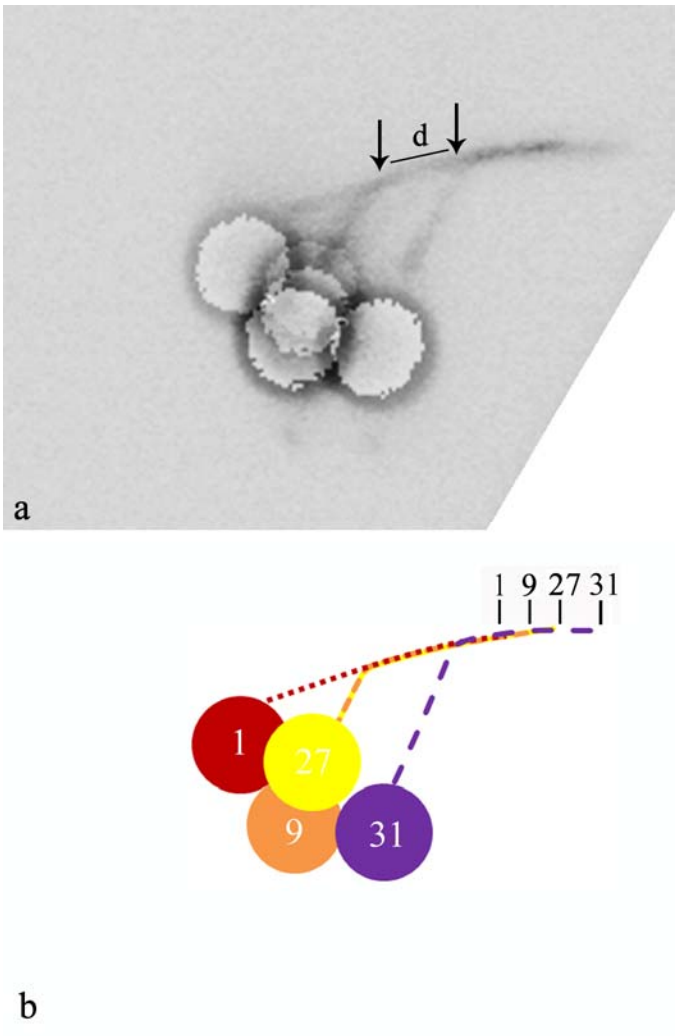

FIG. 3. (a) Overlay of 5 frames from Fig. 2 to show the distance *d* between two anchor points. (b) Schematic of frames 1,9,27 and 31 (color online). The position of the leading end of the microtubule is marked by the frame number in the upper right side of the diagram.

The distance between anchor points was measured for injected kinesin concentrations of 8.3, 3.9, and 1.5μg/mL. The location of each anchor point was determined by postprocessing of stored images. The distance between two anchor points was taken as *d*, the distance between functional motors.

B. Dependence of <*d*> on σ_{nom}: experiments and model

The average values of *d* for injected kinesin concentrations of 8.3, 3.9 and 1.5 μg/ml (σ_{nom} = 508, 240, 90 μm^{-2}) were 1.66 ± 0.18, 2.40 ± 0.10 and 3.97 ± 0.50 μm (mean ± SEM). The DHL theory proposes that $\langle d \rangle \sim \sigma^{-1}$ in regime i and $\langle d \rangle \sim \sigma^{-2/5}$ in regime ii. We first tested whether either prediction was met by plotting *log* <*d*> against *log* σ_{nom}. The slope of the best line through our data was of 0.5 ± 0.1 (data not shown). This suggested that our experiments correspond to Regime ii. To further test this, we plotted $\langle d \rangle$ against σ_{nom} and superimposed least-squares best-fit curves corresponding to $\langle d \rangle \sim \sigma^{-1}$ and $\langle d \rangle \sim \sigma^{-2/5}$ (Fig. 4). The curve $\langle d \rangle \sim \sigma^{-2/5}$ fits the data well, indicating that our experiments fall into Regime ii.

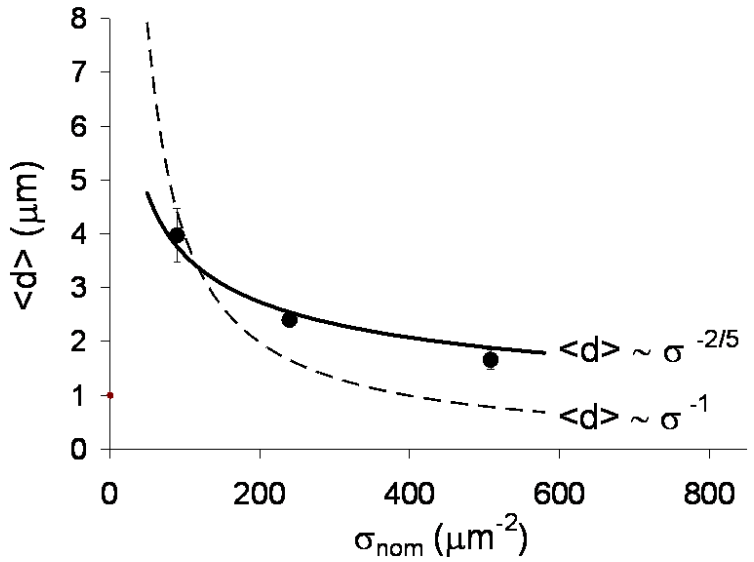

FIG. 4. The average distance between anchor points plotted against σ_{nom}. Also shown are best-fit curves for $\langle d \rangle \sim \sigma^{-1}$ and $\langle d \rangle \sim \sigma^{-2/5}$, corresponding to Regimes i and ii.

C. The distribution of *d*

To further test how a gliding microtubule tip finds additional motors, we computed histograms of the measured values of *d* and compared them to the distributions predicted by an extension of the DHL model (Fig. 5). For [KHC] = 3.9 and 8.3 μg/mL, the histograms appear to be right skewed. However, we note that the bin at 0.5 μm may be empty only because detachments with $d < 0.75$μm could not be observed.

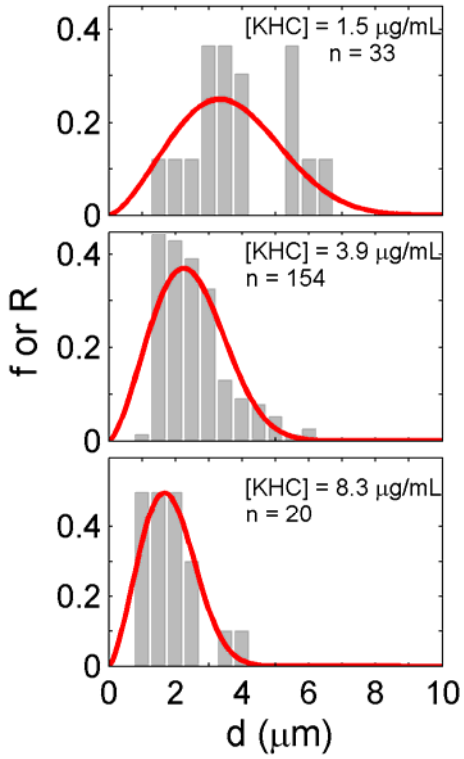

FIG. 5. Measured and modeled distributions of the distance *d*. The experimental data are shown as normalized histogram frequencies *f* for a bin width of 0.5µm. The curves (red online) show the normalized probability distribution *R* calculated by our extension of the DHL model (Eq. 9). The number of experimental observations in the histograms was 33, 154, and 20 for [KHC] = 1.5, 3.9, and 8.3 µg/mL respectively.

Following standard treatments of mean-free path [32], we extended the DHL model for regime ii to give distributions in *d*, as follows. Let *P(x)* be the probability that the leading tip

of the moving microtubule reaches *x* without meeting a motor, and let *Q(x)dx* be the probability that the tip finds a motor between *x* and *x* + *dx.* In the spirit of the DHL model,

$$Q(x)dx = 2\sigma z(x)dx \qquad (3)$$

where z(x) is the half-width of the searchable area (Fig 1).

Knowing *Q(x)*, one can obtain *P(x)*:

$$P(x+dx) = P(x)(1-Q(x)dx)\,. \qquad (4)$$

Since $P(x+dx) = P(x) + \frac{dP}{dx}dx,$ this reduces to

$$\frac{dP}{P} = -Q(x)dx \qquad (5)$$

Integrating and applying the boundary condition $P(0) = 1$, one obtains

$$P(x) = \exp[-2\sigma\int_0^x z(x')dx']\,. \qquad (6)$$

Knowing *P(x)* and *Q(x)*, we can determine *R(x) dx*, the probability that the tip meets a motor when its length falls between *x* and *x* + *dx:*

$$R(x)dx = P(x)Q(x)dx\,. \qquad (7)$$

R(x) is the distribution we will compare to the measured histogram.

To determine a numerical value for *R(x)*, we need *z(x)*, the amplitude of the diffusive side-to-side fluctuations of the tip in the potential well which is defined by the flexural rigidity and the length of the tip. For a round rod of length *L* with one end fixed and the other free in a bath of temperature *T* with negligible density and viscosity, the mean-square amplitude of mode *i* is given by

$$\left\langle z_i^2 \right\rangle = \frac{12 k_B T L^3}{3EI\alpha_i^4} \qquad (8)$$

where E is the elastic modulus, $I = \int y^2 dA$ is the cross-sectional y moment of inertia of a slice across the beam with unit mass per unit area, and k_B is Boltzmann's constant [33, 34]. The mode amplitude factor α_i is 1.88 for the lowest-frequency mode which dominates the side-to-side sweeping of the tip. The product EI, often called the "flexural rigidity", equals 2.2 x 10^{-23} Nm^2 for taxol-stabilized microtubules [35]. Setting T = 295K, the square root of Eq. (8) yields $z_{rms} = 7.7L^{1.5}$ with z and L expressed in meters. Thus Eqs.3 and 6 give $Q(x) = 15.4\sigma x^{3/2}$ and $P(x) = \exp[-6.2\sigma x^{5/2}]$ where σ is in m^{-2} and x is in m. The distribution $R(x)$ is then given by

$$R(x) = \exp[-6.2\sigma x^{5/2}]\{15.4\sigma x^{3/2}\}. \qquad (9)$$

Thus σ is the only variable still to be determined.

Our kinesin concentrations were less than 10 μg/mL or 43 nM and our measured values of d all exceeded 1 μm or 125 tubulin dimers along a protofilament. Also, our injected concentrations are much less than 200 nM, the K_D for the surface binding of a kinesin similar to ours [36]. As a consequence of their separation, it is unlikely that the kinesin molecules could interact with one another while binding to the casein-coated surface. Thus, we expect σ to vary linearly with σ_{nom} in our experiments. Then $\sigma = f\sigma_{nom}$, where f is the "functional fraction" of kinesin. To find f for our experiments, we computed $R(x)$ and $\langle d \rangle$ for the model with f between 0.01 and 0.10. For each value of f, we computed the goodness of fit

$\chi^2 = \sum_{i=1}^{3} (\langle d_{obs} \rangle - \langle d_{model} \rangle)^2$ between the observed values of $\langle d \rangle$ and the values of $\langle d \rangle$ predicted by the model. A plot of χ^2 against f was parabolic with a well-defined minimum at $f = 0.047 \pm 0.004$. The resultant values of σ for our three kinesin concentrations were 4.5 ± 0.4, 12 ± 1, and $25 \pm 2\ \mu m^{-2}$.

Although the value of *f* may appear to be low, we note that it describes the fraction of motors that are functional after binding to the casein surface and within the assumptions of the DHL model. Hunt, Gittes and Howard suggest that *f* is less than 0.1 [20] because many molecules may not bind with a favorable orientation. In addition, our estimate assumes, with the DHL model, that all potentially functional motors within the area swept by the microtubule tip will in fact bind.

The distributions *R* predicted by the model could then be computed from Eq. (9). These distributions are shown as continuous curves in Fig. 5, superposed on the experimental histograms. The widths and shapes of the curves for the model are in good accord with the measured distributions, especially for the middle kinesin concentration, for which 154 experimental points were obtained. The values of *d*, σ_{nom}, and σ which we have determined for our kinesin concentrations are summarized in Table 1 below:

TABLE 1. The distance between anchor points, nominal surface density, and functional surface density at 3 kinesin concentrations.

kinesin concentration (μg/mL)	$\langle d \rangle$ (μm)	nominal surface density σ_{nom} (μm^{-2})	functional surface density σ (μm^{-2})
8.3	1.66 ± 0.18 (n=20)	508	25 ± 2
3.9	2.40 ± 0.10 (n=154)	240	12 ± 1
1.5	3.97 ± 0.50 (n=30)	90	4.5 ± 0.4

D. The shape of bends around anchor points

Anchor points were evident in our experiments as localized zones at which the radius of curvature of the microtubule was much smaller than one might expect if the microtubule behaved like a simple cantilever with a small force applied to its free end [34]. To be quantitative about this visual impression, we evaluated the radius of curvature for the microtubules at anchor points. The measured values were 1.07 ± 0.10 μm (n=22) for microtubules bent 45-135º and 0.77 ± 0.05 μm (n=7) for microtubules bent 180º around an anchor point (Fig 4). For comparison, the radius of curvature of long taxol-stabilized microtubules under thermal forces is between 450 and 6000 μm. [35, 37-39] . It is apparent that the curvature distribution[40] for the microtubule shown in Figure 6 would be bimodal.

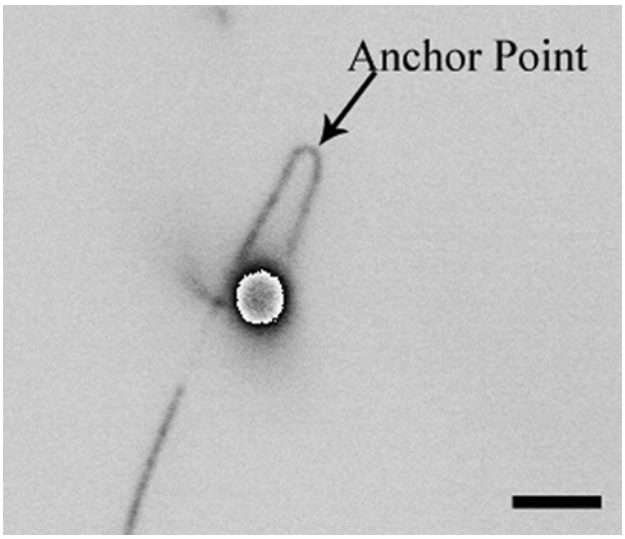

FIG. 6. A microtubule with a 180° bend caused by a 4pN force acting on the bead. This force is directed toward the bottom of the image. The scale bar is 5 microns.

The torque and work done by the magnetic force in our experiments can be estimated by consideration of Fig. 7.

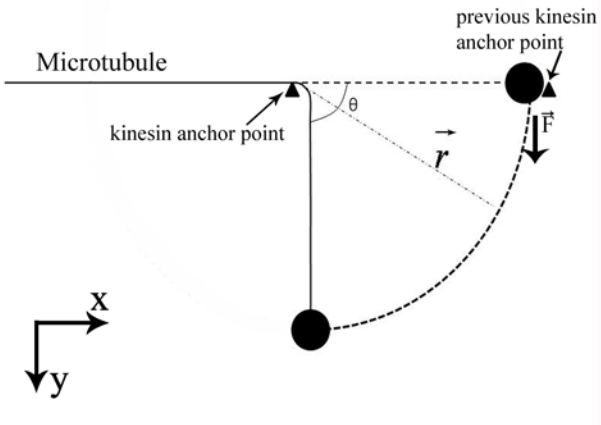

FIG. 7**.** Diagram of the motion of a bead after detachment. The force **F** on the bead provides an initial bending moment *rF*. As the bead moves down, the microtubule sweeps

through an angle θ. At $\theta = \pi/2$, the bending moment goes to zero. The deformation of the microtubule is localized near the anchor point, in contrast to the deformation of a simple cantilever with a small load applied to its tip.

The work W done by F is:

$$W = \int_0^{\theta} r \times F d\theta' \tag{13}$$

If the integral is evaluated with r=5μm, $|F|$=4*pN* and $\theta = \frac{\pi}{2}$, Eq. (13) yields $W \approx 2 \times 10^{-17}$ J. This is about 5000 times $k_B T$ at 300K.

The large value of W, the large initial bending moment (20 pN·μm), and the fact that the microtubule bends sharply at the anchor point but appears stiff elsewhere, all suggest that microtubule models appropriate for small deflections of homogeneous cantilevers [35, 41, 42] are inappropriate here. The sharp local bend of the microtubule is probably better understood within a two-state molecular model of microtubule bending proposed by Heussinger et al. [26, 27] There, the microtubule is modeled as a bundle of cross-linked tubulin protofilaments, with each protofilament represented as a wormlike chain[26, 43]. Each protofilament has high stiffness relative to the soft crosslinks between protofilaments. Under small loads perpendicular to the long axis of the microtubule, the protofilaments remain coupled to one another, but at high perpendicular load (our situation) the protofilaments become uncoupled and slide past each other. For a 13 protofilament microtubule, the ratio of the bending rigidity

for small loads to that at large loads is estimated to be 35[27]. In our experiments, both states apparently occur within different regions of the same microtubule (Figure 6).

The small radius of curvature of microtubules which we observed at anchor points most likely arose from the simultaneous presence of a large bending moment and a kinesin molecule at the point of highest bending stress.

III. DISCUSSION

The binding points between a microtubule and the kinesin-coated surface over which it glides were revealed by a sharp bend in the normally stiff microtubule. The location of the bend was fixed on the surface; the microtubule continued to glide past the binding point. This showed that the bend was not a consequence of an imperfection in the microtubule structure. A microtubule became detached from its binding points if a sustained transverse force of 4-15 pN was applied to its (+) end. After detaching from one point, the next binding point was revealed. We associate each binding point with a functional kinesin motor.

Many aspects of the detachment process are still unclear. Do detachments occur at a particular point in the biochemical cycles of the heads? Do they depend on ATP concentration? Do they depend on the rate of force application? We did determine that, at constant kinesin concentration (3.9μg/mL, $\sigma=12\ \mu m^{-2}$), the average time interval between detachments decreased with increasing force on the bead: 0.81s for 5.9pN, 0.52s for 12pN, and 0.49s for 18 pN.

Several groups have studied the deflection of the path of gliding microtubules by transverse electric fields, with the goal of using molecular motors as shuttles in

nanotechnology applications. Kim *et al*. [3, 44] observe that the leading tip because sharply bent under the application of an electric field. They also observe that the deflection increases with lower kinesin surface density and suggest that this arises from a longer free tip length (cantilever length) at lower kinesin concentration, as in the DHL model. Van den Heuvel et al. [6, 25] also studied the deflection of the path of a gliding microtubule subjected to a transverse electric field. They estimate that the length of the deflectable tip in their experiments is approximately 0.10μm. Neither group observed detachment of the leading end from the nearest binding point.

Our measurements of $\langle d \rangle$ immediately provide an approximate value for the number of motors *n* pulling a microtubule of length *L:*

$$n \approx L / \langle d \rangle \tag{14}$$

For a microtubule of length 10μm gliding on a surface coated at our middle kinesin concentration, $\langle d \rangle$ = 2.4μm and thus $n \approx 4$. Only 3 detachments would be required to reach $n = 1$, which is easily identified by the onset of microtubule swiveling. In an earlier study of gliding assays against a viscoelastic load, using the same kinesin preparation used here, we found that the number of kinesins per unit length was 0.35 ± 0.03 μm^{-1} [8]. This corresponds to $\langle d \rangle \approx 2.9 \mu m$. The agreement with values determined here (Table 1) is encouraging.

In extending the DHL model to predict the distribution of *d* (Fig 5), we set the value of the product *EI* of microtubules to 2.2 x 10^{-23} Nm^2 [35]. Some studies suggest that product decreases 10-fold to 2 x 10^{-24} Nm^2 for microtubules of length 3μm or less[3, 45-47]. Eq. (8)

shows that a 10-fold decrease in the product *EI* would increase the width of the search area by a factor of $\sqrt{10}$. Other studies find no length dependence in *EI* [35, 37, 38].

IV CONCLUSIONS

Using video microscopy of fluorescently labeled microtubules with a magnetic bead attached to their (+) ends, we detected binding points of microtubules to a kinesin-coated surface by applying a uniform transverse force of 4-19 pN to the bead. We suggest that each binding point marks the location of a motor. Then the distance between binding points provides a direct measure of the distance *d* between motors. We found that the scaling of $\langle d \rangle$ with surface density σ fitted the predictions of the Duke, Holy, and Liebler model in regime ii, $\langle d \rangle \sim \sigma^{-2/5} p^{1/5}$. The measured distribution of *d* was also found to fit the predictions of the DHL model.

The radius of curvature for our microtubules was large, as expected, except near the anchor point, where it was anomalously small. This is evidence, within a single molecule, for the two distinct states described in a molecular theory of microtubule mechanical properties recently proposed by Heussinger and co-workers[27].

Acknowledgments: We thank Joe Howard for the gift of plasmid pPK113. This work was supported by the Wake Forest University startup grant to Jed C. Macosko and NIH grant NS053493(GH). We thank Jason Gagliano for helpful discussions and preparation of kinesin, and Matthew Steen for assistance with image acquisition software.

SUPPORTING INFORMATION : Two movies are available on EPAPS [31]. In *Popoff_movie_1.avi* a microtubule is gliding at approximately 90º to the magnetic force. The magnetic force was turned on in frame 5. Detachments are visible in frames 29, 39, 42 and 47. The current in the magnet was 1.4A, giving a 4 pN force. Figs. 2 and 3 of the main text were obtained from this movie. The 2.8μm diameter of the bead provides an internal size scale.

Popoff_movie_2.avi shows a microtubule gliding approximately 45º from the direction of the magnetic force. A current of 2A is turned on at frame 46, applying a 5.5pN force. A detachment event can be observed in frame 56. The microtubule swivels after frame 56. This shows that the microtubule is bound by a single kinesin[21]. The 2.8μm bead diameter provides an internal length scale.

REFERENCES

[1] J. M. Scholey, *Motility Assays for Motor Proteins* (Academic Press, New York, 1993).
[2] J. Howard, *Mechanics of Motor Proteins and the Cytoskeleton* (Sinauer Associates, Sunderland, MA, 2001).
[3] T. Kim, M.-T. Kao, E. F. Hasselbrink, and E. Meyhoefer, Biophys. J. **94**, 3880 (2008).
[4] T. Korten, and S. Diez, Lab Chip **2008**, 1441 (2008).

[5] T. Nitta, A. Tanahashi, Y. Obara, M. Hirano, M. Rasumova, M. Regnier, and H. Hess, Nano Letters **8**, 2305 (2008).
[6] M. G. van den Heuvel, M. P. deGraaff, and C. Decker, Science **312**, 910 (2006).
[7] C. Leduc, F. Ruhnow, J. Howard, and S. Diez, Proceedings of the National Academy of Sciences **104**, 10847 (2007).
[8] J. Gagliano, M. Walb, B. Blaker, J. Macosko, and G. Holzwarth, European Biophysics Journal **39**, 801 (2010).
[9] S. M. Block, C. L. Asbury, J. W. Shaevitz, and M. J. Lang, Proceedings of the National Academy of Sciences of the United States of America **100**, 2351 (2003).
[10] M. Vershinin, B. C. Carter, D. S. Rasafsky, S. J. King, and S. P. Gross, Proceedings of the National Academy of Sciences **104**, 87 (2007).
[11] J. Beeg, S. Klumpp, R. Dimova, R. S. Gracia, E. Unger, and R. Lipowsky, Biophys. J. **94**, 532 (2008).
[12] J. A. Laib, J. A. Marin, R. A. Bloodgood, and W. H. Guilford, Proceedings of the National Academy of Sciences **106**, 3190 (2009).
[13] G. T. Shubeita, S. L. Tran, J. Xu, M. Vershinin, S. Cermelli, S. L. Cotton, M. A. Welte, and S. P. Gross, Cell **135**, 1098 (2008).
[14] M. A. Welte, S. P. Gross, M. Postner, S. M. Block, and E. F. Wieschaus, Cell **92**, 547 (1998).
[15] D. B. Hill, M. J. Plaza, K. D. Bonin, and G. Holzwarth, European Biophysics Journal **33**, 623 (2004).
[16] C. Kural, H. Kim, S. Syed, G. Goshima, V. I. Gelfand, and P. R. Selvin, Science **308**, 1469 (2005).
[17] V. Levi, A. S. Serpinskaya, E. Gratton, and V. Gelfand, Biophys. J. **90**, 318 (2006).
[18] Y. Shtridelman, G. Holzwarth, C. Bauer, N. Gassman, D. DeWitt, and J. Macosko, Cellular and Molecular Bioengineering **2**, 190 (2009).
[19] P. Bieling, I. A. Telley, J. Piehler, and T. Surrey, EMBO Journal **9**, 1121 (2008).
[20] A. J. Hunt, F. Gittes, and J. Howard, Biophys. J. **67**, 766 (1994).
[21] J. Howard, A. J. Hunt, and S. Baek, in *Motility Assays For Motor Proteins*, edited by J. M. Scholey (Academic Press, Inc, San Diego, California, 1993), pp. 139.
[22] P. Katira, A. Agarwal, T. Fischer, H.-Y. Chen, X. Jiang, J. Lahann, and H. Hess, Advanced Materials **19**, 3171 (2007).
[23] T. Duke, T. E. Holy, and S. Leibler, Physical Review Letters **74**, 330 (1995).
[24] T. L. Fallesen, D. B. Hill, M. Steen, J. C. Macosko, K. D. Bonin, and G. M. Holzwarth, Review of Scientific Instruments **81**, 074303 (2010).
[25] M. G. L. Van den Heuvel, M. P. de Graaff, and C. Dekker, Proceedings of the National Academy of Sciences **105**, 7941 (2008).
[26] C. Heussinger, M. Bathe, and E. Frey, Physical Review Letters **99**, 048101 (2007).
[27] C. Heussinger, F. Schüller, and E. Frey, Physical Review E **81**, 021904 (2010).
[28] D. L. Coy, M. Wagenbach, and J. Howard, Journal of Biological Chemistry **274**, 3667 (1999).
[29] A. A. Hyman, Journal of Cell Science **Supplement 14**, 125 (1991).
[30] R. D. Vale, F. Malik, and D. Brown, The Journal of Cell Biology **119**, 1589 (1992).
[31] EPAPS, 2010).

[32] F. Reif, *Fundamentals of Statistical and Thermal Physics* (McGraw-Hill book Company, New York, 1965), p. p 463 ff.
[33] H.-J. Butt, and M. Jaschke, Nanotechnology **6**, 1 (1995).
[34] M. Paz, and W. Leigh, *Structural Dynamics: Theory and Computation* (Springer, New York, 2004), pp. p 535.
[35] F. Gittes, B. Mickey, J. Nettleton, and J. Howard, The Journal of Cell Biology **120**, 923 (1993).
[36] A. Seitz, and T. Surrey, EMBO Journal **25**, 267 (2006).
[37] M. Kikumoto, M. Kurachi, V. Tosa, and H. Tashiro, Biophys. J. **90**, 1687 (2006).
[38] P. Venier, A. C. Maggs, M. F. Carlier, and D. Pantaloni, Journal of Biological Chemistry **269**, 13353 (1994).
[39] B. Mickey, and J. Howard, The Journal of Cell Biology **130**, 909 (1995).
[40] A. D. Bicek, E. Tuezel, D. Kroll, and D. J. Odde, Methods in Cell Biology **82**, 237 (2007).
[41] R. P. Feynman, R. B. Leighton, and M. Sands, *The Feyman Lectures on Physics* (Addison-Wesley, Reading, MA, 1964), Vol. II, pp. p.38.
[42] L. D. Landau, and E. M. Lifshitz, *Theory of Elasticity* (Pergamon, London, 1959), Vol. 7, p. 134.
[43] M. Bathe, C. Heussinger, M. M. A. E. Claessens, A. R. Bausch, and E. Frey, Biophys. J. **94**, 2955 (2008).
[44] T. Kim, M.-T. Kao, E. F. Hasselbrink, and E. Meyhoefer, Nano Letters **7**, 211 (2006).
[45] M. Kurachi, M. Hoshi, and H. Tashiro, Cell Motility and the Cytoskeleton **30**, 221 (1995).
[46] F. Pampaloni, G. Lattanzi, J. Alexandr, S. Thomas, F. Erwin, and E.-L. Florin, Proceedings of the National Academy of Sciences **103**, 10248 (2006).
[47] T. Takasone, S. Juodkazis, Y. Kawagishi, A. Yamaguchi, S. Matsuo, H. Sakakibara, H. Nakayama, and H. Miisawa, Japanese Journal of Applied Physics **41**, 3015 (2002).